Journal of Applied Polymer Science

Development of a conjugated polyaniline incorporated electrospun poly(vinylidene fluoride-*co*-hexafluoropropylene) composite membrane electrolyte for high performance dye-sensitized solar cells

Vijayakumar Elayappan,[1] Vignesh Murugadoss,[1] Subramania Angaiah,[1] Zhaofu Fei,[2] Paul J. Dyson[2]

[1]Electrochemical Energy Research Lab, Centre for Nanoscience and Technology, Pondicherry University, Puducherry 605 014, India

[2]Institut des Sciences et Ingénierie Chimiques, Ecole Polytechnique Fédérale de Lausanne (EPFL) CH-1015, Lausanne, Switzerland

Correspondence to: S. Angaiah (E-mail: a.subramania@gmail.com)

ABSTRACT: Different weight percentage (2, 3, 4, and 5 wt %) of polyaniline (PANI) were incorporated into electrospun poly(vinylidene fluoride-*co*-hexafluoropropylene) (PVdF-HFP) composite membranes (esCPMs). The regular morphology, molecular structure, crystallinity, porosity, electrolyte uptake, and leakage of the composite membranes were examined. The esCPMs were activated in liquid electrolyte containing 0.5 M LiI, 0.05 M I_2, and 0.5 M 4-*tert*-butylpyridine and 0.5 M 1-*butyl*-3-methylimidazoliun iodide in acetonitrile to afford electrospun PVdF-HFP/PANI composite membrane electrolytes (esCPMEs). The influence of different wt % of PANI on the esCPMEs was studied by electrochemical impedance measurements and Tafel polarization studies. The photovoltaic performance of a dye-sensitized solar cell assembled using 3 wt % PANI incorporated esCPME exhibits a higher power conversion efficiency of 7.20% than that assembled using esPME ($\eta = 6.42\%$). © 2015 Wiley Periodicals, Inc. J. Appl. Polym. Sci. **2015**, *132*, 42777.

KEYWORDS: composites; electrochemistry; fibers; membranes; photochemistry

Received 2 June 2015; accepted 23 July 2015
DOI: 10.1002/app.42777

INTRODUCTION

Dye-sensitized solar cells (DSSCs) are among the most extensively investigated devices that provide a high light-to-electric energy conversion devices.[1] One of the critical components of DSSCs is the electrolyte which contains redox couple, often I^-/I_3^- to meditate the dye regeneration process and the devices containing liquid electrolytes have achieved high light to power conversion efficiency (PCE) of about 12%.[2] Nevertheless, solvent evaporation and leakage of liquid electrolytes desorption of weakly adsorbed dyes and corrosion of electrodes can be problematic. It would therefore be advantageous to replace the liquid electrolytes. Among the various alternatives such as ionic liquids,[3,4] P-type semiconductors,[5] ionic conducting polymers,[6] organic hole transport polymers,[7] and polymer gel electrolytes,[8] polymer membrane electrolyte containing I^-/I_3^- redox couple attracts great attention due to its higher ionic conductivity and an excellent long-term stability towards DSSCs. Recently, electrospun polymer membrane containing ionic liquid has attracted remarkable interest.[9–12] Among the techniques available for the preparation of polymer membranes, electrospinning is a simple and versatile, and has a high degree of reproducibility. Electrospun membranes provide better electrolyte uptake because of their three-dimensional network with interconnected pores. Hence, the ionic conductivity of electrospun polymer membrane electrolyte is usually high compared with that of other conventional polymer membrane electrolyte. These interconnected pores are able to trap the liquid electrolyte and consequently, the resulting esPMEs appears to act as a liquid as well as a gel electrolyte. Conductive polymers such as polyaniline (PANI), polypyrrole, polythiophene, polyacetylene, and so on, show potential applications in DSSCs because of their unique properties, such as inexpensiveness, high-conductivity, good stability, and catalytic activity for I_3^- reduction.[13–18] Among various conducting polymers, PANI is an excellent one with more advantages such as low cost, easy synthesis, high-conductivity, good environmental stability, and interesting redox properties.[19–21] Herein, we describe an approach to improve ion transport in polymer membrane electrolyte by inclusion of the conjugated PANI due to its controllable electrical conductivity, environmental stability, and relevant redox properties.[20,22] Indeed, a conducting PANI incorporated polymer gel electrolyte was reported recently that exhibits good electrical conduction

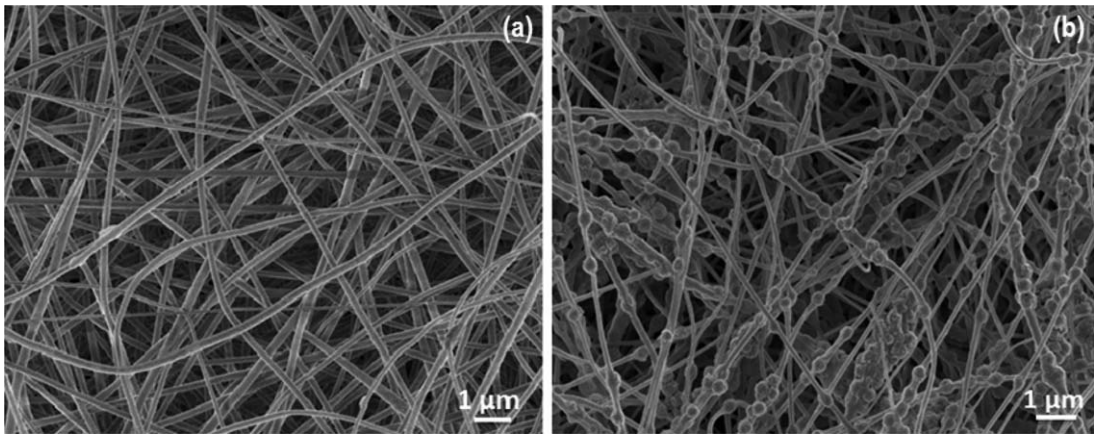

Figure 1. FE-SEM images of (a) esPM and (b) 3 wt % PANI incorporated esCPM.

behavior.[23] In presence of PANI, the superior electrocatalytic activity towards I^-/I_3^- redox reaction and an increased ionic conductivity and electron transport were observed.[24] The inclusion of PANI in a polymer gel was shown to accelerate the mobility of charge carriers in the electrolyte so that the triodide can migrate rapidly to the Pt-coated counter electrode and be efficiently reduced at the counter electrode, instead of the recombination with the titania anode.[25] In addition, the integration of conjugated structure of PANI can shorten the charge diffusion path length and more importantly, the conjugated PANI structure participates in the dye regeneration by hole injection into the PANI.[19] Among the numerous polymer matrices studied, the vinylidene fluoride-hexafluoropropylene copolymer is of considerable interest because it has relatively lower crystallinity compared with other polymer matrices.[26] However, the PANI incorporated electrospun poly(vinylidene fluoride-*co*-hexafluoropropylene) (PVdF-HFP) membrane electrolyte for DSSC has not been studied yet. The electrospun polymer membrane is activated by liquid electrolyte as they provide the advantages of nonvolatility, thermal stability, as well as high ionic conductivity. Hence, in this investigation, different weight percentage of PANI incorporated electrospun PVdF-HFP composite membranes are activated with a liquid electrolyte and the influence of PANI on photovoltaic performance are studied in detail.

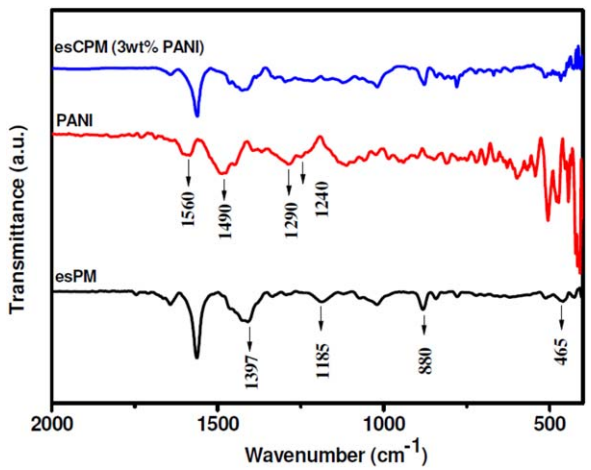

Figure 2. FTIR spectra of esPM, PANI and esCPM (3 wt % PANI). [Color figure can be viewed in the online issue, which is available at wileyonlinelibrary.com.]

EXPERIMENTAL

Materials

PANI nanoparticles were prepared as per the literature.[6] Acetone and *N*, *N*′-dimethylacetamide were procured from Merck India Ltd. Lithium iodide, iodide, 4-*tert*-butylpyridine, and acetonitrile were procured from Sigma Aldrich and PVdF-HFP from Arkema (Kynar flex 2801). All these chemicals are analytical grade and used as received without any further purification.

Preparation of esCPMs

The electrospun PVdF-HFP/PANI composite membranes were prepared using 16 wt % of PVdF-HFP solution in a mixture of acetone/*N*,*N*′-dimethyl acetamide (7 : 3 wt %) containing different weight percentage of PANI (2, 3, 4, and 5 wt %) with respective to PVdF-HFP. The resulting polymer solution was supplied to the stainless steel syringe needle (27 G) using a syringe pump at a flow rate of 0.5 mL/h. The electrospinning was carried out at the voltage of 19 kV and the distance between the collector and tip of the needle was kept at 12 cm. The resulting nanofibrous membrane was vacuum dried at 80°C for 12 h to remove residual solvent. The thickness of electrospun PVdF-HFP composite membranes (esCPMs) was reduced from about 30 to 20 μm by hot pressing.[10]

Characterization of esCPMs

The surface morphology of esCPMs was examined by field emission scanning electron microscopy (FE-SEM; Model: JSM-7600F). Structural characterization of esCPMs was studied by X-ray diffraction (Rigaku, Ultima IV) with nickel-filtered Cu-Kα radiation in the range of 20°–80° with an increment of 0.05°. Thermal behavior of esCPMs[27] was measured using differential scanning calorimetric (DSC; TA Instruments, Model: Q600 SDT) at a heating rate of 10°C/min under nitrogen atmosphere in the temperature range of 30–200°C.

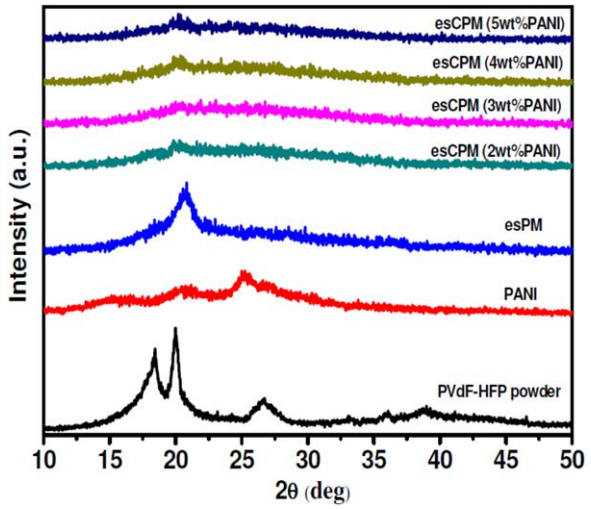

Figure 3. XRD patterns of PVdF-HFP powder, PANI, esPM, and different wt % PANI incorporated esCPMs. [Color figure can be viewed in the online issue, which is available at wileyonlinelibrary.com.]

The crystallinity (X_c) of the esCPMs was calculated as follows[8]

$$X_c(\%) = \frac{\Delta H_m^{\text{sample}}}{\Delta H_m^*} \times 100 \quad (1)$$

where $\Delta H_m^{\text{sample}}$ is the heat of melting of the sample and ΔH_m^* is the crystalline melting heat of PVdF, 104.7 J/g.

The porosity (P) of esCPMs was determined by weighing the membrane with and without 1-butanol from the following equation[28]

$$P = \frac{m_a/\rho_a}{m_a/\rho_a + m_p/\rho_p} \quad (2)$$

where m_a is the weight of esCPM after impregnation with 1-butanol, m_p is the weight of esCPM before impregnation with 1-butanol, and ρ_a and ρ_p are density of 1-butanol and the dried esCPM, respectively.

To measure the electrolyte uptake of both esPM and esCPMs, the membranes were soaked in the liquid electrolyte for 24 h. They were then taken out from the liquid electrolyte solution and the excess electrolyte solution on the membrane was wiped off using whatman filter paper. Electrolyte uptake (U) was estimated using

$$U\ (\%) = [(m - m_\circ)/m_\circ] \times 100 \quad (3)$$

where, m and m_o are the mass of wet and dry electrospun esCPMs, respectively.[29]

The leakage of electrolyte was calculated using

$$R = \frac{M_{\text{PE}}}{M_{\text{PE, saturated}}} \quad (4)$$

where, R is the relative absorption ratio of liquid electrolyte, $M_{\text{PE,-saturated}}$ is the mass of esCPME when the membrane is fully saturated with the liquid electrolyte and M_{PE} is the mass of esCPME after a time interval when the saturated polymer membrane electrolyte is squeezed by pressing it between the filter papers.[30]

The different esCPMs were soaked in the liquid electrolyte to form their corresponding esCPMEs. The ionic conductivity (σ) of resulting esCPMEs was measured by sandwiching the esCPME between two stainless steel blocking electrodes and recorded their AC-impedance spectra (Biologic Model: VSP) at 25°C. The ionic conductivity of esCPME was calculated using the equation[31]

$$\sigma = \ell/RA \quad (5)$$

where ℓ is the polymer membrane thickness, A is the area of the electrospun PVdF-HFP/PANI composite membrane electrolyte, and R is the bulk resistance. The frequency limit was set between 1 mHz and 100 KHz with an AC amplitude of 10 mV. The thickness (ℓ) of esCPME was determined using a digital micrometer (Mitutoyo, Japan) and was found to be 20 μm. The area (A) of the polymer membrane electrolyte was 1 cm^2.

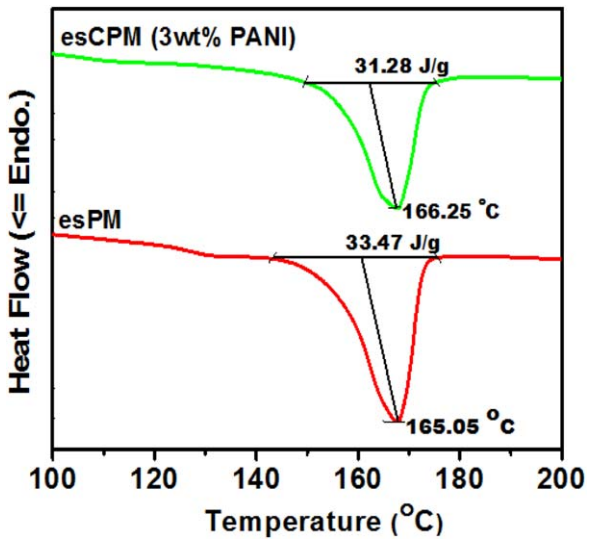

Figure 4. DSC curves of esPM and 3 wt % PANI incorporated esCPM. [Color figure can be viewed in the online issue, which is available at wileyonlinelibrary.com.]

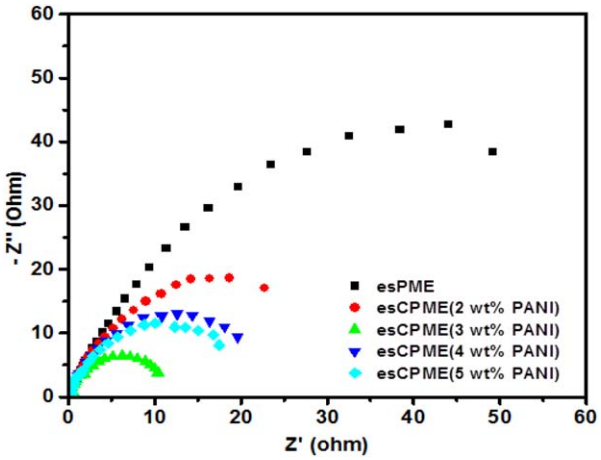

Figure 5. Nyquist plots for esPME and different wt % of PANI incorporated esCPMEs on ionic conductivity. [Color figure can be viewed in the online issue, which is available at wileyonlinelibrary.com.]

Table I. Influence of Different wt % of PANI Incorporated esCPME on ionic Conductivity, Electrolyte Uptake, and Porosity

Electrolyte	σ ($\times 10^{-3}$ S cm^{-1})	U (%)	P (%)
esPME	05.83	340	89.0
esCPME (2 wt % PANI)	24.55	422	90.0
esCPME (3 wt % PANI)	31.44	446	92.7
esCPME (4 wt % PANI)	27.47	429	91.1
esCPME (5 wt % PANI)	22.72	414	89.4

DSSC Fabrication

A detailed procedure to assemble the DSSC was reported previously.[32] The DSSC containing the esCPME was assembled by sandwiching a slice of esCPME between a dye-sensitized std. TiO_2 photoanode and standard Pt counter electrode. The dye adsorbed TiO_2 photoanode and Pt counter electrode were assembled using a 60 μm thick hot melt thermoplastic sealer (Surlyn).[33] A required amount of the electrolyte containing 0.5 M LiI, 0.05 M I_2 and 0.5 M 4-tertbutylpyridine and 0.5 M 1-*butyl*-3-methylimidazoliun iodide in acetonitrile[10] was injected into the clamped electrodes through one of two small holes drilled in the counter electrode. Similarly, a control DSSC based on esPME was also assembled for comparison.

Photovoltaic Performance of DSSCs

The photovoltaic performance of DSSCs was determined by using a calibrated AM 1.5 solar simulator (Newport, Oriel instruments, Model: 67005) with a light intensity of 100 mW cm^{-2} and a computer controlled digital source meter (Keithley, model: 2420). I–V measurements were carried out on the DSSCs after an aging period of 24 h. The DSSCs were stored in a desiccator and measurements were made for every 48 h to determine their long-term stability. Photoelectrochemical parameters including the fill factor (FF) and PCE (η) were calculated using the following equations[32]

$$\eta\ (\%) = \frac{V_{\max} J_{\max}}{P_{in}} \times 100 = \frac{V_{oc} J_{sc} FF}{P_{in}} \times 100 \quad (6)$$

$$FF = \frac{V_{\max} J_{\max}}{V_{oc} J_{sc}} \quad (7)$$

where J_{sc} is the short-circuit current density (mA cm^{-2}), V_{oc} is the open-circuit voltage (V), P_{in} is the incident light power (mW cm^{-2}), and J_{max} and V_{max} are the current density (mA cm^{-2}) and voltage (V) in the J-V curves, respectively, at the point of maximum power output. All the fabrication steps and characterization measurements were carried out in an ambient environment without a protective atmosphere. The photovoltaic parameter values were obtained from the average values of three DSSC devices.

RESULTS AND DISCUSSION

Characterization of esCPMs and esCPMEs

The morphologies of the esPM and esCPM (3 wt % of PANI) are shown in Figure 1(a,b). They comprise fibers with a uniform size distribution and well defined structure. The average fiber diameter of esPM is 300–400 nm and the esCPM is 300–350 nm. Notably, the FE-SEM image of the esCPM shows additional particles that correspond to incorporated PANI nanoparticles. The addition of PANI nanoparticles to the PVdF-HFP solution increases the net charge density carried by the moving jet. The increased net charge increases the force exerted in the jet that forms the balls of PANI in the nanofibers.

The electrospun fibrous membrane has a porous structure and the esCPM has a maximum porosity and an electrolyte uptake of 92.71% and 446%, respectively, being higher than the esPM (82% and 340%). The higher porosity of esCPM is reflected in higher uptake of the electrolyte solution. Importantly, the absorbed liquid electrolyte is well retained in the esCPMEs and is showing a very low leakage of 0.2%. This is due to the interconnected pores present in the nanofibrous membrane can ensure the long term stability of DSSCs operations.

The Fourier transformed infrared spectra of PVdF-HFP, PANI and PVdF-HFP/PANI matrix are shown in Figure 2. The peaks at about 1397, 880, and 465 cm^{-1} are due to the C-F_2 bending, wagging, and stretching vibrations and the peak at 1185 cm^{-1} is due to C—C bond of PVdF.[9] For PANI, the peaks at 1560 and

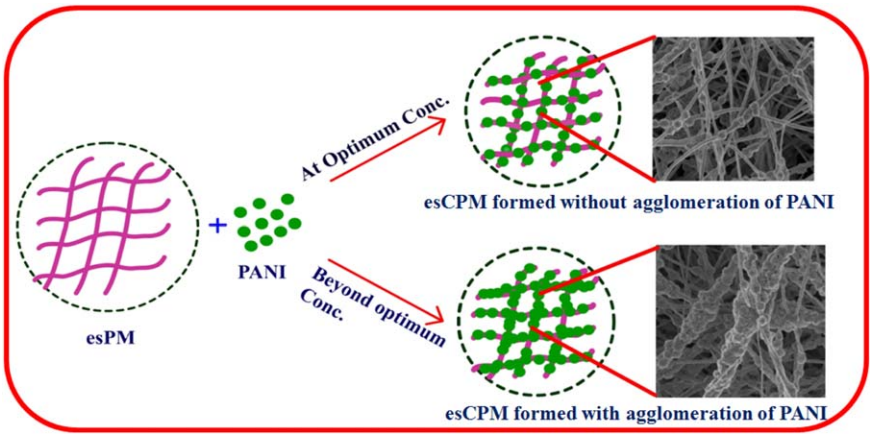

Figure 6. Schematic representation of the esCPM formation. [Color figure can be viewed in the online issue, which is available at wileyonlinelibrary.com.]

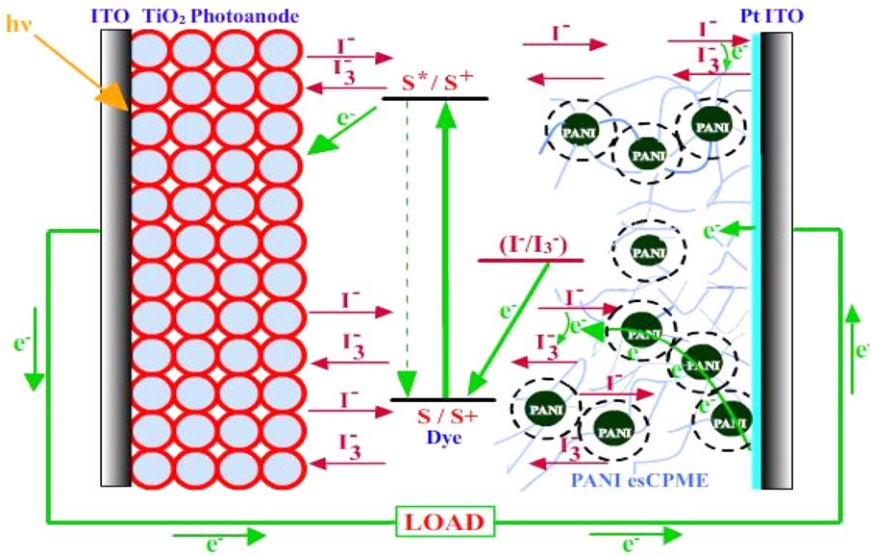

Figure 7. Schematic illustration of ion transport mechanism for DSSC containing 3 wt % of PANI incorporated esCPME. [Color figure can be viewed in the online issue, which is available at wileyonlinelibrary.com.]

1490 cm^{-1} are ascribed to the stretching of quinoid and benzenoid rings, respectively.[34] The peak at around 1290 cm^{-1} arises from the C—N stretching of a secondary aromatic amine. The peak at around 1240 cm^{-1} can be interpreted as C—N^+ stretching vibration of polaron structure.[35,36] No shift in peaks was observed in esCPM indicating that there is no conjugate bond or interaction between PVDF-HFP and PANI nanoparticles. It reveals that the PANI nanoparticles are physically embedded in the host esCPM and there is no complex formation between PVdF-HFP and PANI.

The XRD patterns of PVdF-HFP powder, PANI, esPM, and different wt % of PANI containing esCPMs are shown in Figure 3. The XRD pattern of PANI exhibits a semi-crystalline structure with a characteristic broad peak at $2\theta = 25.5°$ corresponding to the (110) lattice plane.[6] In the XRD pattern of PVdF-HFP powder, the major peaks at 18.2° and 20.0° correspond to (100) and (020) crystalline phases, respectively.[37,38] In case of esPMs the intensity of peak weakening indicate decrease in crystallinity. The intensity of peak decreased obviously, when PANI nanoparticles are added. This indicates that the addition of PANI further reduced the degree of crystallinity of electrospun PVdF-HFP membrane, which is responsible for the enhancement of ionic conductivity. The lowest crystallinity observed for 3 wt % of PANI incorporated esCPM. However, beyond 3 wt % of PANI incorporated esCPM, the crystallinity again increased due to the agglomeration of PANI nanoparticles.

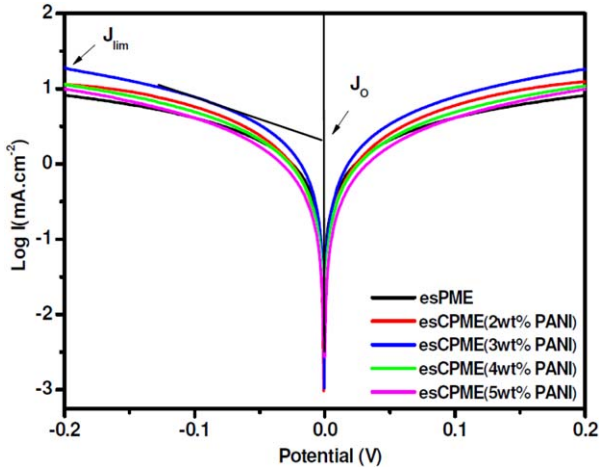

Figure 8. Tafel polarization curves of the symmetrical cells assembled with esPME and different wt % of PANI incorporated esCPMEs. [Color figure can be viewed in the online issue, which is available at wileyonlinelibrary.com.]

DSC curves of esPM and 3 wt % of PANI incorporated esCPM are shown in Figure 4. It reveals one endothermic peak at about 165°C for both materials. This result indicates that the addition of PANI considerably improve the thermal properties of esCPM.[8,39] The 3 wt % esCPM has the lower crystallinity (29.87%) than that of esPM (31.97%) which are determined using equation (1) showing these results are consistent with the results of XRD analysis.

The ionic conductivity of esCPMEs soaked in the liquid electrolyte was determined by AC-impedance spectroscopy at 25°C is shown in Figure 5 (Table I). Among the studied esCPMEs, 3 wt % of PANI incorporated esCPME has the highest ionic conductivity value of 31.44×10^{-3} S cm^{-1} than the value obtained for esPME (5.83×10^{-3} S cm^{-1}). The incorporation of PANI in esCPME adds electron transfer channels, which facilitates the electrical conduction of reflux electron that accelerate the redox reaction kinetics.[24] The homogenous attachment of PANI nanoparticles facilitates the segmental mobility of polymer chains that helps in the dissociation of ions in the polymer matrix, which increases the ionic conductivity of the electrolyte. However, on increasing the PANI content beyond 3 wt % esCPM formed with the agglomeration of PANI which hinder the segmental mobility in the polymer matrix of esCPME, thereby reducing the ionic conductivity (Figure 6).[40,41]

Table II. Photovoltaic Performance of DSSCs Containing esPME and 3 wt % PANI Incorporated esCPME

Electrolyte	J_{sc} (mA cm^{-2})	V_{oc} (V)	FF	Efficiency (%)
esPME	13.10	0.71	69	6.42
esCPME(3 wt % PANI)	14.30	0.72	70	7.20

Figure 7 illustrates the conceptual mechanism of the improvement of ion transport in DSSC using 3 wt % of PANI incorporated esCPME. The incorporated PANI nanoparticles act as bridge that favor the electron conduction thereby enhancing the redox reaction I^-/I_3^- due to their excellent electrical conductivity. Thus, the 3 wt % of PANI incorporated esCPME extending the reduction site of I^-/I_3^- from pt counter electrode/esCPME interface to the interconnected three dimensional network of esCPME. Furthermore, the PANI nanoparticles interact with the ionic liquid electrolyte form space charge layer thereby accelerating the ion mobility within esCPME.[42]

Tafel-polarization measurements are used to further confirm the electrocatalytic activity of esCPMEs using a dummy cell comprising FTO/Pt/esCPME/Pt/FTO. Figure 8 shows the Tafel curves of the symmetrical cell assembled with esCPMEs. The curve at very high potential may be attributed to the limiting diffusion zone, which depends on the transport of triiodide and iodide in the electrolyte. The curve at very low potential is the polarization zone which arises from the electrochemical reaction. The steeper slope for the anodic or cathodic branches in Tafel polarization curve indicates a higher exchange current density (J_0) on the electrode and better catalytic activity towards triiodide reduction. The slope for the anodic or cathodic branch represents exchange current density ($J_0 = RT/nFR_{ct}$). It is apparent that the esCPME (3 wt % PANI) has the maximum J_0 and therefore, higher charge-transfer ability than other concentrations of esCPMEs. Additionally, the intersection of cathodic

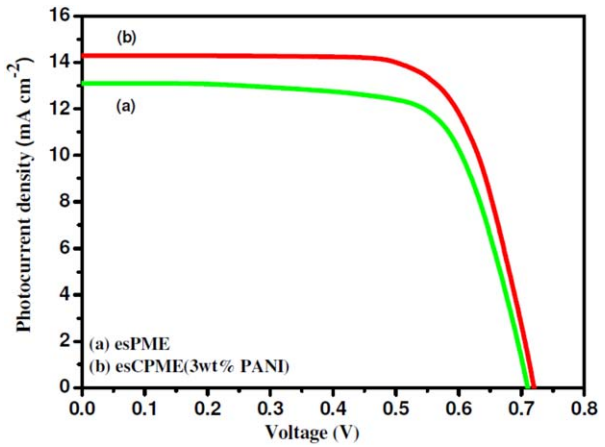

Figure 9. Photocurrent density-voltage (J-V) curves for DSSCs based on (a) esPME and (b) 3 wt % PANI incorporated esCPME. [Color figure can be viewed in the online issue, which is available at wileyonlinelibrary.com.]

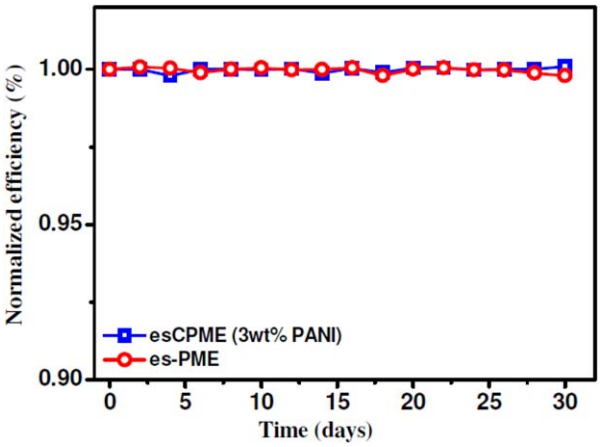

Figure 10. Normalized light-to-electricity conversion efficiency of the DSSCs containing (a) esPME and (b) 3 wt % PANI incorporated esCPME. [Color figure can be viewed in the online issue, which is available at wileyonlinelibrary.com.]

branch with the *y*-axis is a limiting diffusion current density ($J_{lim} = 2nFCDn/l$) parameter dependent on the diffusion coefficient of I^-/I_3^- redox couples.[19] The extracted J_{lim} and diffusion coefficient of redox species (D_n) for esCPME (3 wt % PANI) is much higher than those of esPME, indicating that the resultant ionic conductivity is significantly elevated. Furthermore, 3 wt % PANI incorporated esCPME showed the highest electrocatalytic activity for I_3^- reduction, and consequently increase the short circuit current of DSSC which enhanced the PCE.

Photovoltaic Performance of DSSCs

DSSCs containing both the esPME and esCPME were assembled as described previously.[43] Photocurrent density-voltage (J-V) curves were obtained at a light intensity of 100 mW cm^{-2} under standard global AM 1.5 irradiation (Figure 9; Table II). The DSSC assembled with 3 wt % PANI incorporated esCPME provides an energy conversion efficiency of 7.20%, which is higher than that DSSC assembled with the esPME which has PCE of 6.42%. The PANI incorporated esCPME leads to the decreased dark current and increased the light current which are beneficial for increase of FF values.[25] The higher PCE of the DSSC containing the esCPME may be attributed to their ionic conductivity, which increase the mobility of charge carriers in the electrolyte, that is, I_3^- can be transported to the Pt coated counter electrode more rapidly and reduced their recombination at the TiO_2 photoanode. Thus, the electrocatalytic nature and reduced charge diffusion path length due to incorporated PANI onto esCPME, synergistically increase the J_{sc} value and thereby increase PCE of the DSSC.[19]

The stability of DSSCs assembled with both esPME and esCPME was studied over a period of 30 days (Figure 10). Both DSSCs retain about 99% of their initial value. Notably, no decay was observed in the overall PCE of both the DSSCs. The three dimensional interconnected pore structure of the electrospun polymer membrane helps to maintain the liquid electrolyte from evaporation thereby ensures the durability of DSSCs. This might be due to their three dimensional network with interconnected pores which is composed of a number of channels (micro pores) present in the electrospun polymer matrix to entrap large quantity of the

liquid electrolyte, thereby preventing leakage of the liquid electrolyte containing I^-/I_3^- redox couple. Thus, both the esPME and esCPME appear to promote interfacial contact between the dye-adsorbed TiO_2 electrode and the Pt counter electrode, which help to give more stable photovoltaic performance.

CONCLUSION

PANI incorporated esCPMEs can be prepared successfully by electrospinning technique and compared with esPME. The esCPMEs showed superior ionic conductivity. A DSSC assembled using esCPME (containing 3 wt % PANI) has a PCE of 7.20% at an illumination intensity of 100 mW cm^{-2}, which is higher than that of observed esPME ($\eta = 6.42\%$). The incorporation of PANI in esCPME reduced the charge transfer resistance which accelerates the I^-/I_3^- redox reaction. This enhanced the J_{sc} value and thereby increases the PCE of the DSSC. Thus, the DSSC assembled using the 3 wt % PANI incorporated esCPME is a promising candidate for DSSC with long durability.

ACKNOWLEDGMENTS

The authors thank the CSIR (Ref. No.01/2359/10/EMR-II) New Delhi for the financial support and also the CIF of Pondicherry University for extending the instrumentation facilities.

REFERENCES

1. O'Regan, B.; Grätzel, M. *Nature* **1991**, *353*, 737.
2. Yella, A.; Lee, H.-W.; Tsao, H. N.; Yi, C.; Chandiran, A. K.; Nazeeruddin, M. K.; Diau, E. W.-G.; Yeh, C.-Y.; Zakeeruddin, S. M.; Grätzel, M. *Science* **2011**, *334*, 629.
3. Park, S.-H.; Won, D.-H.; Choi, H.-J.; Hwang, W.-P.; Jang, S.; Kim, J.-H.; Jeong, S.-H.; Kim, J.-U.; Lee, J.-K.; Kim, M.-R. *Sol. Energy Mater. Sol. Cells* **2011**, *95*, 296.
4. Lau, G. P. S.; Tsao, H. N.; Zakeeruddin, S. M.; Grätzel, M.; Dyson, P. J. *Appl. Mater. Interfaces* **2014**, *6*, 13571.
5. Bandara, J.; Yasomanee, J. *Semicond. Sci. Technol.* **2007**, *22*, 20.
6. Ayad, M.; El-Hefnawy, G.; Zaghlol, S. *Chem. Eng. J.* **2013**, *217*, 460.
7. Wang, H.-J.; Tzeng, J.-Y.; Chou, C.-W.; Huang, C.-Y.; Lee, R.-H.; Jeng, R.-J. *Polym. Chem.* **2013**, *4*, 506.
8. Subramania, A.; Sundaram, N. T. K.; Priya, A. R. S.; Kumar, G. V. *J. Memb. Sci.* **2007**, *294*, 8.
9. Vijayakumar, E.; Subramania, A.; Fei, Z.; Dyson, P. J. *RSC Adv.* **2015**, *5*, 52026.
10. Vijayakumar, E.; Subramania, A.; Fei, Z.; Dyson, P. J. *J. Appl. Polym. Sci.* **2015**, *132*, 42032.
11. Wu, J.; Lan, Z.; Lin, J.; Huang, M.; Huang, Y.; Fan, L.; Luo, G. *Chem. Rev.* **2015**, *115*, 2136.
12. Fei, Z.; Kuang, D.; Zhao, D.; Klein, C.; Ang, H. *Synthesis.* **2006**, *45*, 1.
13. Tai, Q.; Chen, B.; Guo, F.; Xu, S.; Hu, H.; Sebo, B.; Zhao, X. Z. *ACS Nano* **2011**, *5*, 3795.
14. Tang, Q.; Cai, H.; Yuan, S.; Wang, X. *J. Mater. Chem. A* **2013**, 317.
15. Li, Q.; Wu, J.; Tang, Q.; Lan, Z.; Li, P.; Lin, J.; Fan, L. *Electrochem. Commun.* **2008**, *10*, 1299.
16. Ghani, S.; Sharif, R.; Bashir, S.; Zaidi, A. A.; Rafique, M. S.; Ashraf, A.; Shahzadi, S.; Rafique, S.; Kamboh, A. H. *J Power Sources* **2015**, *282*, 416.
17. Han, R.; Lu, S.; Wang, Y.; Zhang, X.; Wu, Q.; He, T. *Electrochim. Acta* **2015**, *173*, 796.
18. Chang, L.-Y.; Li, C.-T.; Li, Y.-Y.; Lee, C.-P.; Yeh, M.-H.; Ho, K.-C.; Lin, J.-J. *Electrochim. Acta* **2015**, *155*, 263.
19. Duan, Y.; Tang, Q.; Chen, Y.; Zhao, Z.; Lv, Y.; Hou, M.; Yang, P.; He, B.; Yu, L. *J. Mater. Chem. A Mater. Energy Sustain.* **2015**, *3*, 5368.
20. Lee, J.-K.; Nath, N. C. D.; Cha, E.-H.; Sarker, S.; Park, H.-S.; Jeong, W.-S.; Hong, S.-H.; Lee, J.-J. *Bull. Korean Chem. Soc.* **2010**, *31*, 3411.
21. Li, Q.; Chen, X.; Tang, Q.; Cai, H.; Qin, Y.; He, B.; Li, M.; Jin, S.; Liu, Z. *J. Power Sources* **2014**, *248*, 923.
22. Wang, P.; Tan, K. L.; Kang, E. T.; Neoh, K. G. *Appl. Surf. Sci.* **2002**, *193*, 36.
23. Li, Q.; Tang, Q.; Lin, L.; Chen, X.; Chen, H.; Chu, L.; Xu, H.; Li, M.; Qin, Y.; He, B. *J. Power Sources* **2014**, *245*, 468.
24. Tang, Z.; Wu, J.; Liu, Q.; Zheng, M.; Tang, Q.; Lan, Z.; Lin, J. *J. Power Sources* **2012**, *203*, 282.
25. Liu, Q.; Wu, J.; Lan, Z.; Zheng, M.; Yue, G.; Lin, J.; Huang, M. *Polym. Eng. Sci.* **2014**, 1.
26. Xiao, W.; Miao, C.; Yin, X.; Zheng, Y.; Tian, M.; Li, H.; Mei, P. *J. Power Sources* **2014**, *252*, 14.
27. Hsu, Y.-C.; Tseng, L.-C.; Lee, R.-H. *J. Polym. Sci. Part B Polym. Phys.* **2014**, *52*, 321.
28. Kim, J. R.; Choi, S. W.; Jo, S. M.; Lee, W. S.; Kim, B. C. *J. Electrochem. Soc.* **2005**, *152*, A295–A300.
29. Kim, J.-U.; Park, S.-H.; Choi, H.-J.; Lee, W.-K.; Lee, J.-K.; Kim, M.-R. *Sol. Energy Mater. Sol. Cells* **2009**, *93*, 803.
30. Angulakshmi, N.; Stephan, A. M. *Electrochim. Acta* **2014**, *127*, 167.
31. Ahn, S. K.; Ban, T.; Sakthivel, P.; Lee, J. W.; Gal, Y.-S.; Lee, J.-K.; Kim, M.-R.; Jin, S.-H. *ACS Appl. Mater. Interfaces* **2012**, *4*, 2096.
32. Priya, A. R. S.; Subramania, A.; Jung, Y.-S.; Kim, K.-J. *Langmuir* **2008**, *24*, 9816.
33. Vijayakumar, E.; Pratheep, P.; Sivasankar, N.; Karthick, S. N.; Subramania, A. *Appl. Phys. A.* **2015**, 10.1007/s00339-015-9306-x.
34. Bavio, M. A.; Acosta, G. G.; Kessler, T. *J. Power Sources* **2014**, *245*, 475.
35. Nath, A. K.; Kumar, A. *Solid State Ionics* **2013**, *253*, 8.
36. Deka, M.; Nath, A. K.; Kumar, A. *J. Memb. Sci.* **2009**, *327*, 188.
37. Kim, K. M.; Park, N.-G.; Ryu, K. S.; Chang, S. H. *Polymer* **2002**, *43*, 3951.

38. Ulaganathan, M.; Nithya, R.; Rajendran, S.; Raghu, S. *Solid State Ionics* **2012**, *218*, 7.

39. Cao, J.; Wang, L.; Fang, M.; He, X.; Li, J.; Gao, J.; Deng, L.; Wang, J.; Chen, H. *J. Power Sources* **2014**, *246*, 499.

40. Nath, B. C.; Gogoi, B.; Boruah, M.; Sharma, S.; Khannam, M.; Ahmed, G. A.; Dolui, S. K. *Electrochim. Acta* **2014**, *146*, 106.

41. Chan, Y.-F.; Wang, C.-C.; Chen, C.-Y. *J. Mater. Chem. A* **2013**, *1*, 5479.

42. Mohan, V. M.; Murakami, K.; Kono, A.; Shimomura, M. *J. Mater. Chem. A* **2013**, *1*, 7399.

43. Subramania, A.; Vijayakumar, E.; Sivasankar, N.; Sathiya Priya, A. R.; Kim, K.-J. *Ionics* **2013**, *19*, 1649.